High-Precision Timing of the Crab Pulsar using the 42-ft Telescope at Jodrell Bank

Third Year Lab Report

Amrit Bath: 10899510
Department of Physics and Astronomy, University of Manchester
(Experiment performed in collaboration with Jade Huang: 10639013)
(Dated: April 19, 2025)

This report investigates the spin properties of the Crab Pulsar (PSR B0531+21) using observational data collected from the 42-ft radio telescope at Jodrell Bank Observatory. The pulsar's spin period was found to be $P = 0.0338390995 \pm 7 \times 10^{-10}$ s, and period derivative $\dot{P} = (4.2 \pm 0.1) \times 10^{-13}$ from de-dispersion, barycentric corrections and residual analysis. These were used to calculate a characteristic age of $\tau = 1274 \pm 30$ yrs, a surface magnetic field of $B = (3.82 \pm 0.09) \times 10^{12}$ G, and an estimated distance of 1880 ± 10 pc. The uncertainties reflect statistical variation in residual alignment. The Period is not consistent with literature findings, however all other calculations are.

1. INTRODUCTION

Pulsars are the remnants of massive stars, typically those with masses between 8 and 20 solar masses, which undergo core-collapse supernovae at the end of their life cycles. When nuclear fusion is no longer able to support the star against its own gravity, the core implodes, causing high-energy particle collisions of protons and electrons into neutrons. The result is an extraordinarily dense object supported by neutron degeneracy pressure, a quantum mechanical force that arises due to the Pauli exclusion principle [1]. Due to conservation of angular momentum, the collapse of the progenitor star's core into a compact neutron star leads to an immense increase in rotation rate. A slowly rotating star will transform into an object spinning up to several times per second, with the fastest known pulsars rotating over 700 times per second [2]. At the same time, the magnetic field intensifies due to intense compression of magnetic flux during collapse, often reaching 10^8 to 10^{15} G. This causes beams of electromagnetic radiation to sweep through space akin to lighthouse beams. If these beams intersect with Earth, they can be detected as regular pulses [3]. The Crab Pulsar (PSR B0531+21) is one of the most well studied pulsars. Located at the centre of the Crab Nebula, at a distance of 1.9kpc, it is the product of a supernova recorded in 1054 AD. The energy emitted by the pulsar illuminates the entire supernova remnant, making the Crab Nebula heavily researched [3].

2. THEORY

2.1. Dispersion

Dispersion is a phenomenon where radio waves spread out in a frequency-dependent manner as they travel through the interstellar medium (ISM), which is composed primarily of ionised gas and free electrons. Lower frequency waves are delayed more than higher ones, resulting in a measurable shift across the frequency spectrum. This effect allows astronomers to infer properties of the ISM and accurately time the arrivals of pulsar signals. The correction due to the ISM can be done using a de-dispersion calculation

$$\mathrm{DM} = t_D \times 2.41 \times 10^{-4} \times f^2. \tag{1}$$

Where t_D is the time delay for a signal of frequency f, DM is the dispersion measure, representing the integrated column density of free electrons along the line of sight to the pulsar, and f is the frequency [4]. The DM can be used to find the distance to the pulsar using

$$\mathrm{DM} = \int_{\text{pulsar}}^{\text{Earth}} n_e \, \mathrm{d}l, \tag{2}$$

where n_e is the free electron number density along the line of sight in cm^{-3} and $\mathrm{d}l$ is the infinitesimal path element along the line of sight from the pulsar to the Earth, expressed in parsecs.

2.2. Characteristic Age

The characteristic age of a pulsar, τ, provides an estimate of the time since the pulsar began spinning down, assuming a constant magnetic field and breaking index of three. The braking index characterises how spin rate evolves over time. For ideal magnetic dipole braking, the braking index takes a theoretical value of three, assuming energy loss solely due to electromagnetic radiation from a rotating dipole, based on the standard model of pulsar. The characteristic age is given by

$$\tau = \frac{P}{2\dot{P}} \tag{3}$$

where τ is the characteristic age of the pulsar, P is the spin period and $\dot{P}$ is the period derivative, which measures the rate of change of the period as the pulsar loses energy. This age represents an estimate for the pulsar age, and is particularly useful when historical records of the supernova are unavailable or uncertain [3].

2.3. Magnetic Field Strength

The surface magnetic field strength of a pulsar can be approximated using the dipole radiation model,

$$B = 3.2 \times 10^{19} \sqrt{P\dot{P}} \quad \mathrm{G} \tag{4}$$

where B is the magnetic field at the surface. This expression assumes a rotating magnetic dipole and provides insight into the pulsar's electromagnetic emissions, energy loss rate, and evolutionary stage [2].

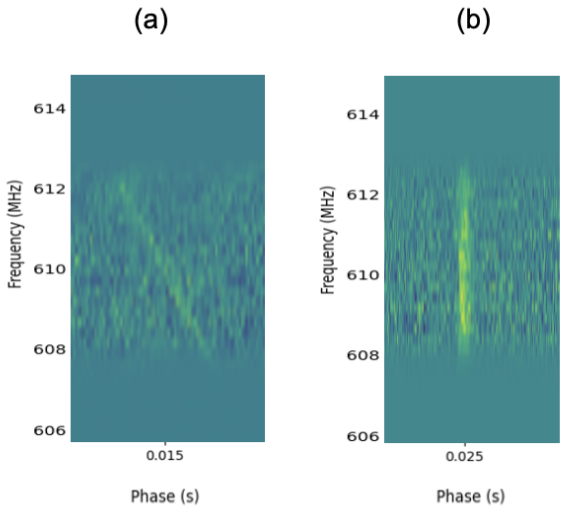

FIG. 1. Sub-figure (a) shows raw data from the pulsar prior to de-dispersion, showing the consequence of dispersion, this has been corrected in Sub-figure (b), where frequencies arrive at the same time.

3. EXPERIMENTAL ANALYSIS

This experiment aimed to investigate the Crab Pulsar by determining its spin period through radio observations, using Fourier techniques and signal processing methods to determine periodicities from noisy astronomical data.

3.1. Data Collection

Observations were conducted using the 42-ft radio telescope at Jodrell Bank Observatory, operating at a central frequency of 611 MHz with a 10 MHz bandwidth. The system utilises a heterodyne receiver, which down-converts the received radio signal to a lower intermediate frequency for efficient digitisation. The signal is then sampled and digitised by a backend processing system, which records the data in standard PSRFITS binary format. Key observational parameters, such as integration time and observing frequency, were configured remotely via a Virtual Network Computing interface. Real-time monitoring was conducted using the Cobra2 system, which displays signal strength, telescope status, and pointing accuracy. The data were later processed in Python-based Jupyter Notebooks for time-of-arrival (TOA) extraction and dispersion analysis.

3.2. De-dispersion of Data

By using Equation 1, we can apply a de-dispersion measure to data collected. Figure 1 shows the frequency data as obtained from the crab pulsar before and after application of the de-dispersion measure. We employed the `differential_evolution` optimiser from the `scipy.optimize` module, allowing us to explore a wide parameter space without relying on a prior DM estimate. Error analysis was conducted in this region by iterating over this process fifty times and taking the average found DM and standard deviation error. This value was to capture variability in the optimisation process, while remaining computationally efficient. The `differential_evolution` optimiser works by taking a random path to find the objective minimum even when bounds and starting positions are the same, meaning that every measurement might yield slight variations. This method produced sharp de-dispersed pulses, robustness and accuracy.

3.3. Location-dependant Delays

Pulsar timing measurements must be corrected for the motion and location of the Earth to ensure that observed time of arrivals (TOAs) reflect intrinsic pulsar behaviour rather than observational effects due to motion of the Earth or observatory. Failure to correct for these effects results in periodic variations in pulse arrival times that mimic timing noise or period drift. To address this, TOAs are converted to the Solar System barycentre frame by applying both the Earth delay and the Roemer delay [5].

The Earth delay corrects for the fact that the observatory is located on Earth's surface, not at its centre. We calculated it by determining the altitude of the pulsar at each TOA using its known sky coordinates and the observatory's location, depending on this altitude, the pulse can arrive slightly earlier or later than it would at the Earth's centre. This delay is given by:

$$\Delta t_{\text{Earth}} = \frac{R_{\text{Earth}} \sin(\epsilon)}{c} \tag{5}$$

where R_{Earth} is the radius of the Earth, ϵ is the pulsar's elevation angle above the local horizon at Jodrell Bank and c is the speed of light. The Roemer delay corrects for delays introduced by the motion of the Earth. As the Earth orbits the Sun, the distance between the pulsar and the telescope changes, causing observed pulse arrival times to be periodically shifted. The total delay due to Earth's motion can be calculated using

$$\Delta t_{\text{Roemer}} = \frac{\vec{r}_{\oplus} \cdot \hat{n}}{c}. \tag{6}$$

Here, $\vec{r}_{\oplus}$ is the position vector of the Earth relative to the Solar System barycentre, $\hat{n}$ is the unit vector pointing from the observer to the pulsar. This is on the order of several minutes depending on the pulsar's sky position. This delay was calculated for each TOA , using interpolated observatory and solar system positions. Adding both the earth and Roemer delays to the raw TOAs yielded barycentric-corrected arrival times, which were then used for residual analysis and spin-down calculations [6].

3.4. Period and Period Derivative

After applying barycentric corrections to TOAs, the residuals, defined as the difference between the observed and predicted pulse arrival times, can be calculated. These provide insight into the accuracy of the assumed spin period. If the assumed period is incorrect, a clear structure will remain in the residuals, often appearing as linear trends in a sawtooth structure when plotted against corrected TOA or pulse number, as seen in Figure 2.

Ideally, residuals should be flat, indicating that the period model fits the data. However, if a linear trend remains, its gradient can be used to correct the assumed period. Linear regions in the residuals correspond to local deviations in pulse arrival times, which arise from a period estimate that is slightly off. To correct the assumed period P_{guess}, we use the gradient of the residuals g

$$P_{new} = \frac{P_{guess}}{1 - g \times P_{guess}}. \tag{7}$$

Parameter	Experimental Work	Literature Value
Spin Period P (s)	$0.0338390995 \pm 7 \times 10^{-10}$	0.033556602 [7]
Period Derivative $\dot{P}$ (s/s)	$(4.2 \pm 0.1) \times 10^{-13}$	4.209×10^{-13} [7]
Characteristic Age τ (yrs)	1274 ± 30	$\sim$ 971–1264 [3]
Magnetic Field B (G)	$(3.82 \pm 0.09) \times 10^{12}$	3.8×10^{12} [2]
Distance (pc)	1880 ± 10	1900 ± 220 [4]

TABLE I. Summary of measured and derived parameters for the Crab Pulsar. Literature values provided for comparison.

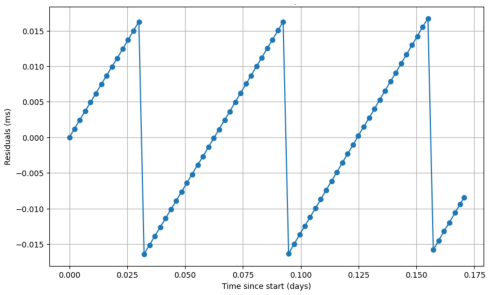

FIG. 2. Residuals from the number of pulses observed plotted against time since the start of observation.

This updated period value can then be used to recompute the residuals and iteratively refine the model until the residuals are flattened.

The spin-down rate, $\dot{P}$, indicates how the pulsar rotation slows over time due to energy losses. It can be found by taking the period found in each weekly measurement for the crab pulsar, and finding the rate of change of this period per measurement. Assuming that there is no $\ddot{P}$, this gives us an estimate into how quickly the crab pulsar loses energy, and therefore the speed at which its spin rate is slowing [8].

4. RESULTS AND ERROR ANALYSIS

The results of the experiment are summarised in Table I. The measured spin period was found to be $P = 0.0338390995 \pm 7 \times 10^{-10}$ s, which deviates slightly from the literature value of 0.033556602 s, likely due to limitations in the residual alignment method, which may introduce systematic bias through pulse broadening or signal-to-noise inconsistencies during sub-integrations.. The period derivative was calculated as $\dot{P} = (4.2 \pm 0.1) \times 10^{-13}$ s/s, consistent with accepted values. However, the low uncertainty suggests potential underestimation of error contributions from instrumental noise and TOA calculation methods.

From these, we computed a characteristic age of $\tau = 1274 \pm 30$ yrs, a surface magnetic field strength of $B = (3.82 \pm 0.09) \times 10^{12}$ G, and an estimated distance to the pulsar of 1880 ± 10 pc. These values are all consistent with those reported in prior literature within uncertainty bounds, with the exception of the period. The deviation in the period likely stems from cumulative observational and analytical uncertainty, particularly due to residual alignment and de-dispersion approximations. The characteristic age being larger than the canonical age of the Crab Pulsar (971 years) is consistent with expectations, as the canonical calculation assumes a constant braking index of three, and the discrepancies likely arise due to an actual non-constant breaking index. The surface magnetic field strength and distance estimates also correspond well to established models of the interstellar medium and pulsar emission physics.

In future research, TOA calculations, derived from template matching, could benefit from more advanced models such as Gaussian interpolation or profile fitting. Future efforts may include longer time-baseline observations to reduce error in $\dot{P}$, applying models accounting for stochastic variations, and refinement of TOA templates to minimise alignment bias.

5. CONCLUSION

This experiment provided investigation into the spin properties of the Crab Pulsar using high-precision timing data from the 42-ft radio telescope at Jodrell Bank. Through Fourier analysis, de-dispersion correction, barycentric TOA alignment and iterative residual finding, key pulsar parameters were determined, including spin period, period derivative, characteristic age, magnetic field strength, and distance. Final measurements, though deviating slightly in spin period from published values, align well with established literature across the remaining parameters. Discrepancies in the spin period highlight the sensitivity of residual alignment techniques and the need for improved error modelling. Future experiments should prioritise increased observation times, refined timing templates, and incorporation of timing noise models to enhance precision.

[1] A. G. Lyne and F. Graham-Smith, *Pulsar Astronomy*, Cambridge Astrophysics Series, Vol. 16 (Cambridge University Press, Cambridge, 1990).

[2] C. G. Bernal, J. A. Rueda, L. Izzo, and R. Negreiros, Frontiers in Astronomy and Space Sciences **11**, 1390597 (2024).

[3] A. Lyne and F. Graham-Smith, in *Pulsar Astronomy*, Cambridge Astrophysics Series (Cambridge University Press, 2012) pp. 117–133.

[4] M. F. Bietenholz, N. Roy, B. M. Gaensler, V. M. Kaspi, M. S. E. Roberts, and B. W. Stappers, The Astrophysical Journal **665**, 618 (2007).

[5] W. M. Folkner, J. G. Williams, and D. H. Boggs, Interplanetary Network Progress Report **42-178**, 1 (2009).

[6] M. A. Seeds and D. E. Backman, *Astronomy: The Solar System and Beyond*, 6th ed. (Cengage Learning, Boston, MA, 2009).

[7] R. N. Manchester, G. B. Hobbs, A. Teoh, and M. Hobbs, The Astronomical Journal **129**, 1993 (2005).

[8] M. M. N. Lewandowska, P. B. Demorest, P. Kilian, and T. H. Hankins, arXiv preprint arXiv:2207.04267 (2022).